International Core Journal of Engineering Volume 11 Issue 3, 2025
ISSN: 2414-1895 DOI: 10.6919/ICJE.202503_11(3).0011

Underwater Acoustic Modulating based on Selective Higher-order Topological Corner States

Haobin Zhang†, Jing Cai, Quanquan Shi, Jiajun Lu

School of Physics and Optoelectronic Engineering, Guangdong University of Technology, Guangzhou 510006, China

†Authors to whom correspondence should be addressed

Abstract

The discovery of Higher-order topological insulators (HTIs) opens new opportunities for the advancement of condensed matter physics and material science topological insulators are a new class of special topological insulators that have been discovered in many classical wave systems in recent years. In this paper, acoustic Dirac degeneracy is achieved by simply rotating scatterers in acoustic crystals, with degeneracy induced accidentally. It provides a new approach for creating higher-order topological insulators in acoustic systems. We observe two kinds of structures and get the gapped one-dimensional (1D) edge states and the gapped zero-dimensional (0D) corner states. At the same time, the edge state is further observed along the interface with two different topological phononic crystals. The topological corner states in this paper enrich the study of higher-order topological insulators and have edge states, which provide a new platform for acoustic systems' transmission properties.

Keywords

Higher-order Topological Insulator; Dirac Degeneracy; Edge States; Corner States.

1. Introduction

Dirac point is a nodal point degeneracy where linear dispersion meets in a two-dimensional band structure [1-3]. Dirac points correspond to massless relativistic particles based on the Dirac equation and can be observed in monolayer graphene. According to the "k·p perturbation theory", the generation of Dirac cones can be deterministic [4] or accidental [5,6]. Deterministic degeneracy is generated by high symmetry and accidental degeneracy results from adjusting the phononic crystal's filling rate or material parameters. The Dirac point is the key to the topological phase transition, and the investigation of topological insulators is developed.

The topological invariants of topological insulators are protected by spatial symmetry, which can be divided into traditional topological insulators and higher-order topological insulators. Traditional topological insulators are also called first-order topological insulators, they have bulk states and edge states, and the dimension of edge states is lower than bulk states. In higher-order topological insulators, the second-order and third-order topological insulators are mainly [7-12]. The two-dimensional (2D) second-order topological insulator is a typical one in higher-order insulator. In a 2D system, compared with traditional topological insulators, the 2D second-order insulator has a zero-dimensional (0D) corner state protected by topology, while the latter does not. Higher-order topological insulators have different bulk-edge correspondences, and such bulk-edge correspondences allow edge states to exist variously. Nowadays, higher-order topological insulators are realized in various classical wave systems, such as optical and acoustic [13-21].

ISSN: 2414-1895 DOI: 10.6919/ICJE.202503_11(3).0011

In previous studies, accidental degeneracy with double [22], triple [23-26], and quadruple [6,27-29] are realized in 2D classical wave systems, by fine-tuning the filling ratio or material parameters of isotropic scatterers. With the accidental degeneracy, topologically protected edge states have been developed [29,30,31], and some of them have been used for wavefront shaping and cloaking [23-25,32]. However, Dirac degeneracy is deterministic in higher-order topological insulator systems, and the accidental degeneracy connected with topological higher-order insulators has not been studied yet.

In this paper, we theoretically design valley-controlled edge transport and higher-order topological corner states in phononic crystals by exploring accidental Dirac degeneracy, higher-order topology, and valley degrees of freedom (d.o.f). We achieve accidental Dirac degeneracy by rotating anisotropic scatterers in a honeycomb phononic cell. The designed phononic crystal with topological edge states verifies topological valley transport. Additionally, the interaction between higher-order topology and valley d.o.f. in 2D phononic crystals enables selective higher-order topological corner states. The valley d.o.f., akin to spin in spintronics, serves as a new information carrier in valleytronics, representing degenerate energy extrema in momentum space [33-37]. This has led to phenomena such as the quantum valley Hall effect and valley filters. [37]. The valley Hall effect allows valley-locked chiral edge states to counter-propagate at domain walls, restraining inter-valley scattering [33]. Finally, we observe strong acoustic transmission along the interface of topologically different acoustic valley Hall insulators, even around structural defects. The proposed phononic crystal shows great potential for use in acoustic transmission devices with arbitrary paths and underwater acoustic sensing.

2. Acoustic Model

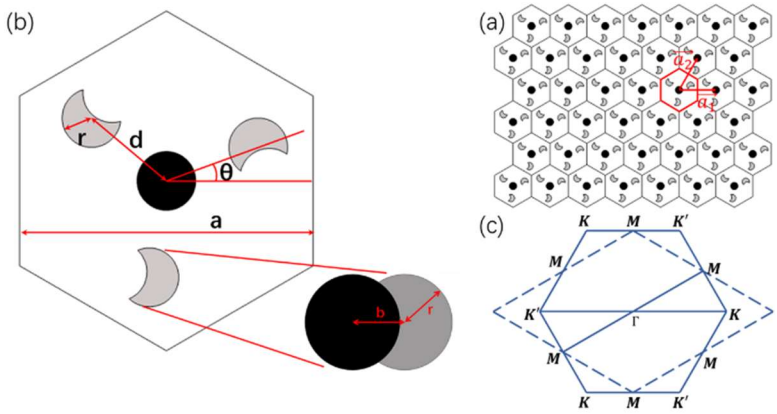

Fig. 1 (a) Acoustic honeycomb structure, the red area represents a cell. A honeycomb phononic crystal composed of three moon-shaped steel scatters indicated by grey, rubber cylinders indicated by black, and water by white. $\overrightarrow{a_1}$ and $\overrightarrow{a_2}$ denote the lattice vectors. (b) The enlarged structure of the unit cell. Inset: The moon-shaped scatterer is obtained by subtracting the black cylinder from the grey one. (c) First Brillouin zone of hexagonal lattice with marked high-symmetry points, which shares the same area with that of rhombic lattice in calculations.

As shown in Fig. 1(a), Our study begins with a two-dimensional acoustic system composed of a hexagonal array of scatterers. Fig. 1(b) shows an enlarged view of a cell (highlighted in red in Fig. 1(a)). Each scatterer consists of a central cylinder surrounded by three moon-shaped columns in water. The lattice constant $a = 4.0$ cm, and the black cylinder has a radius $r = 0.1 * a$. The grey moon-shaped scatterer is formed by subtracting a cylinder of radius r (black) from another cylinder of radius r (grey), with the distance between their centers being $b = 0.11 * a$. The distance between the lattice center and the grey moon-shaped scatterer center is $d = 0.333 * a$. By rotating the three moon-shaped scatterers around the black cylinder's center, characterized by the rotation angle θ. The lattice has a C_3 symmetry at $\theta = 0°$. Changing θ, alters the energy band gap and physical

ISSN: 2414-1895 DOI: 10.6919/ICJE.202503_11(3).0011

properties of the acoustic honeycomb structure, leading to a topological phase transition. Fig. 1(c) shows the first Brillouin zone of a unit cell. Here are the acoustic parameters of the material: the density of soft rubber (respecting black cylinder at the center of the cell) $\rho_1 = 1000\ kg/m^3$, and sound velocity $c_1 = 489.9m/s$; the density of steel (respecting grey moon-shaped scatterers)$\rho_2 = 8000kg/m^3$, sound velocity $c_2 = 5000m/s$; For water, $\rho_3 = 1000\ kg/m^3$, $c_3 = 1482.9\ m/s$. Fig. 1(c) also shows the first Brillouin zone of the hexagonal lattice, which is equivalent to that of the rhombus.

3. Topological Phase Transitions

In this paper, we explore the quantum Valley Hall effect in a honeycomb structure, where rotating scatterers in the cell control the band gap. Fig. 2 shows the dispersion and pressure field profiles of the two eigenstates at the K point with different rotation angles θ. The dispersion of the phononic crystal is illustrated for rotation angles at $\theta = 24.9°$, $-4.57°$ and $-34.2°$, as shown in Figs. 2(a)-(c). When $\theta = -34.2°$, a bandwidth of about 2.2 kHz is obtained in Fig. 2(a). As shown in Fig. 2(b), a twofold Dirac degeneracy forms at points K (K') in the Brillouin zone, closing the band gap when the rotation Angle is $\theta = -4.57°$. As the scatterers continue to rotate clockwise, the band gap reopens in Fig. 2(c).

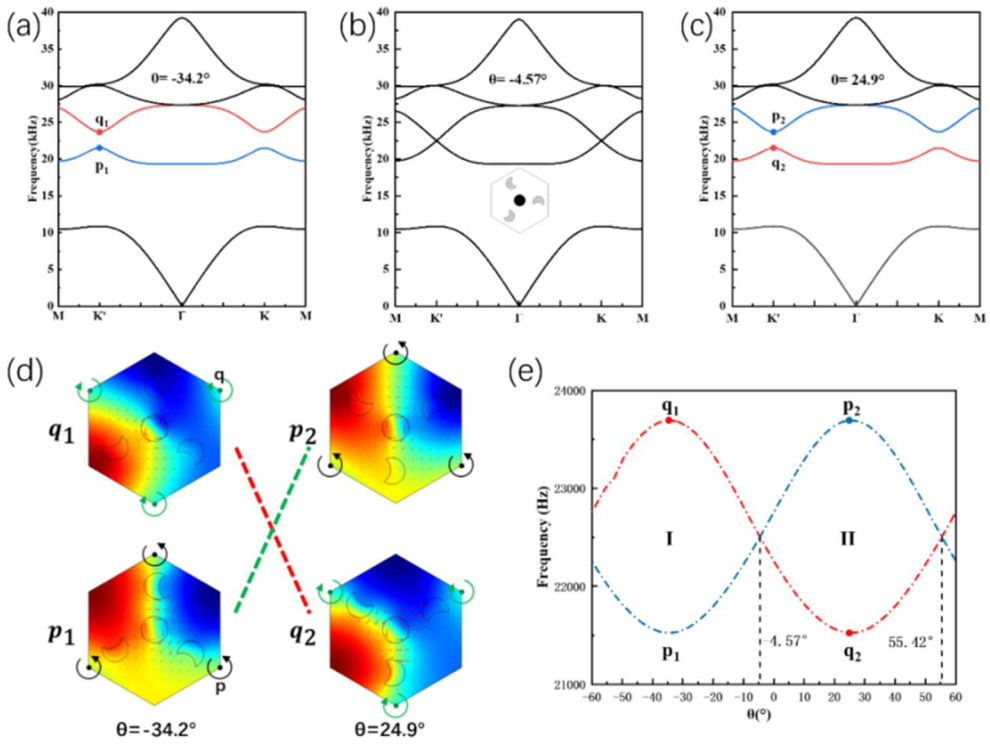

Fig. 2 (a)-(c) Acoustic band structure for phononic cell with $\theta = -34.2°$,$-4.57°$ and $24.9°$ (inset in (b) shows the cell at $\theta = -4.57°$). (d) The sound pressure profiles (and the arrows respecting the Poynting vectors) of the eigenstates at the first two valley states in K point, with $\theta = -34.2°$(left) and $\theta = 24.9°$(right). It shows opposite vortex chirality and witnesses a topological phase transition. (e) The frequencies diagram of phononic cells in the two valleys at K point, with different values of θ. The frequencies of q and p states respect red and blue dotted curves, and the eigenstates exhibited in (d) are also signed in (e).

The pressure field profiles of the two eigenstates at the K point are shown in Fig. 2(d). Green and black arrows and dots denote different chirality and vortex centers, with arrows indicating the

ISSN: 2414-1895 DOI: 10.6919/ICJE.202503_11(3).0011

Poynting vectors (energy flow direction). If + and - are used to represent the counterclockwise and clockwise rotation directions of the vortex and p and q are used to mark the high symmetric points (also referred to as the Wyckoff positions), it can be observed that the $p_1(p_2)$ and $q_1(q_2)$ have opposite vortices. The frequency order of the p and q states is reversed, indicating the typical band inversion associated with topological phase transitions. When the transition angles $\theta = -4.57°$ are crossed, the band inversion is characteristic of topological valley Hall phase transition. Fig. 2(e) shows the corresponding frequencies of the second and third bands of the phononic crystal at point K, which continuously evolve with the rotation angle θ. Since phononic crystals are symmetric C_3, we show a periodicity of $120°$ for the diagram. The band frequencies are the same at $-4.57°$ and $55.42°$, suggesting a valley Hall phase transition due to bandgap closure related to accidental Dirac degeneracy. These transition angles separate two different angular regions, I and II.

4. Topological Edge States of Supercells

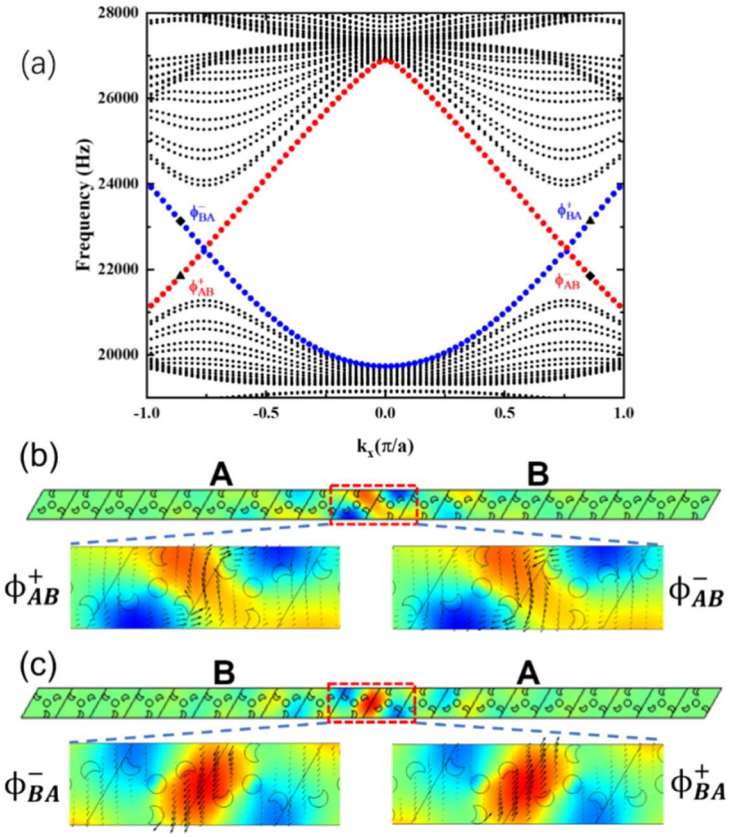

Fig. 3 (a) The projected band structure of the supercell, with dispersions of the edge states (blue and red dots) and bulk states (black dots) constructed by two structures. (b) The pressure and intensity field of the edge states are denoted, respectively, by the rhombic and triangle in red dots as shown in (a). (c) The pressure and intensity field of the edge states are denoted, respectively, by the rhombic and triangle in blue dots as shown in (a).

The formation of edge states arises from the topological valley numbers of different structures on either side of the boundary, with phononic crystals exhibiting distinct valley Hall phases. By combining two phononic crystals with opposite topological phases, we can observe the projected band structure of an A-B supercell, composed of 10 phononic crystals each from regions I and II. Fig. 3 shows this structure, with Floquet periodic boundary conditions along the y-axis and hard sound boundaries on the x-axis. For simplicity, hexagonal cells are replaced with rhombic cells. In Fig. 3(a), the projected band structure along the x-axis is calculated, with the wave vector k on the abscissa and frequency on the ordinate. Black dots indicate bulk states, while red and blue dots represent edge

ISSN: 2414-1895 DOI: 10.6919/ICJE.202503_11(3).0011

states from the K and K' valleys, respectively. The topological band gap ranges from 21.3 kHz to 24.0 kHz, with opposite group velocities for the two interfaces. States $\phi_{AB}^{\pm}$ and $\phi_{BA}^{\pm}$, related to valley-dependent topological edge states, corresponding to the A-B and B-A interfaces. "+" denotes forward-traveling edge states, while "-" indicates backward-traveling ones. Figs. 3(b)-(c) show that the pressure and intensity fields of the edge states are localized at the interface and decay on both sides of the supercell, exhibiting valley pseudospin up and down.

5. Valley-controlled Edge Transport

Valley-controlled edge transport leverages the anti-reflection and robust transport advantages of topological edge states. To observe and verify these properties, we designed two topological acoustic Valley Hall insulators, each sized 20a*20a, as shown in Figs. 4(a)-(b). A point source (red star) is placed on the left side of the junction, with orange and blue parts representing A and B, respectively. The valley-controlled edge propagation of the acoustic wave is illustrated in Figs. 4(c)-(d). When phononic crystals A and B with different Valley Hall phases are arranged as in Fig. 4(a), the insulator supports straight-wave transmission. When A and B form a Z-shaped structure, the acoustic wave flows around corners without reflection.

Fig. 4(d) shows the band gap in the transmittance spectrum for three simulation cases. The black solid line represents the linear transmission path of A-B topological insulators, while the red dotted line represents the Z-type transmission path. The figure demonstrates that the Z-type waveguide transmission efficiency matches well with the linear waveguide transmission efficiency. In contrast, traditional band-gap waveguides with acoustic topological insulators suffer from severe backscattering at sharp bends, significantly reducing transmission efficiency. This verifies the anti-reflection property of valley spin edge propagation.

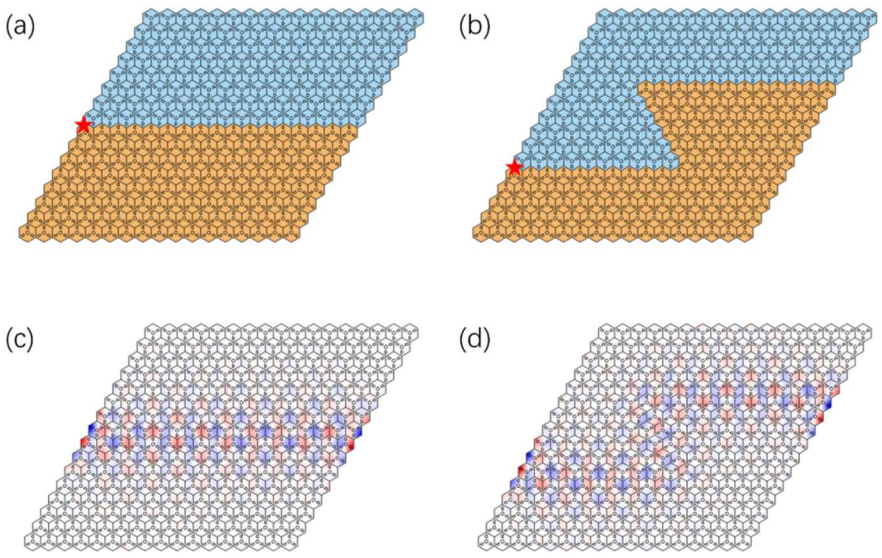

Fig. 4 Valley-controlled edge transport of A-B type interface. (a) and (b) are schematic of the straight and Z-shape transmission. (c) and (d) are the acoustic pressure field distributions at 22107 Hz and 22720 Hz.

6. Topological Corner States in Triangular Structures

A 2D higher-order topological insulator, based on the principle of bulk-edge correspondence, has topology-protected corner states at the edges and corners of a finite structure. However, not all higher-order topological insulators exhibit protected corner states. To study the valley-locking property in our higher-order topological insulator, we designed a triangular structure with 105 cells and a hard

ISSN: 2414-1895 DOI: 10.6919/ICJE.202503_11(3).0011

boundary, as shown in Fig. 5(a). The eigenspectra of this structure, shown in Fig. 5(b), reveal corner states (blue) and edge states (red). Figs. 5(d)-(f) display the bulk state (21499 Hz), edge state (21608 Hz), and corner state (21470 Hz), respectively. When the structure with $\theta = -34.2°$, no corner state appears in the eigenspectra, demonstrating the valley selectivity of the corner state, as shown in Fig. 5(c).

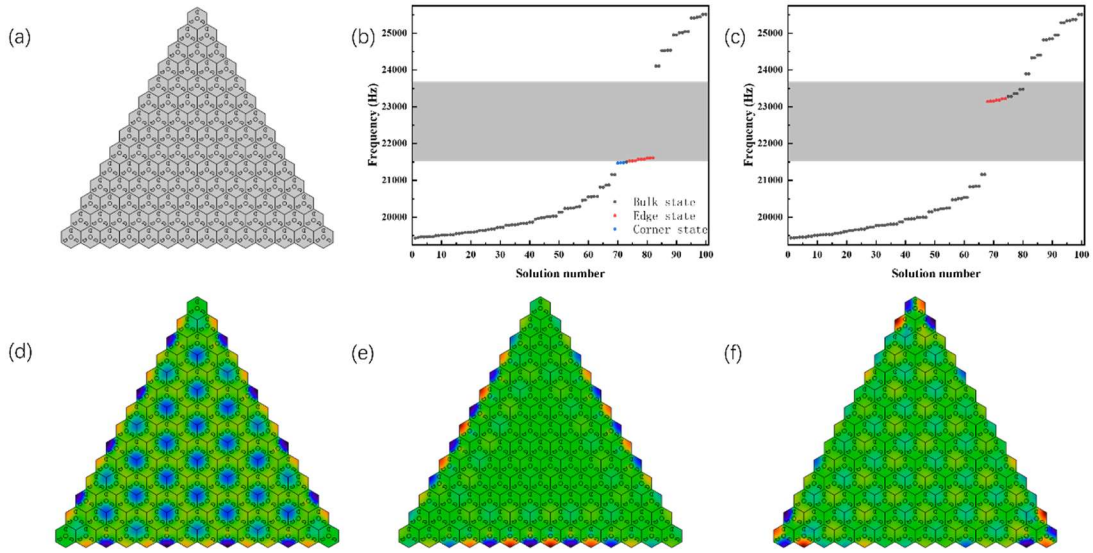

Fig. 5 (a) Triangle honeycomb structure. (b) and (c) are the eigenspectra of the topological and trivial triangle structure; the grey, red, and blue dots correspond to the bulk, edge, and corner state, separately. (d)-(f) The eigenfields distribution of bulk, edge, and corner state at 21499,21608 and 21470 Hz.

7. Topology of Rhombus Structure

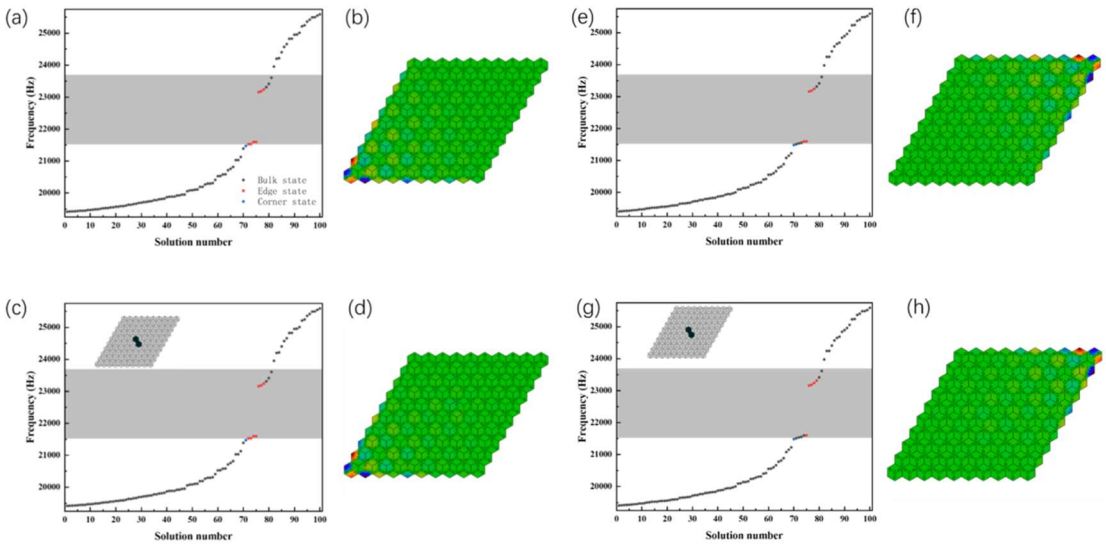

Fig. 6 (a) The eigenspectra of rhombus honeycomb structure at $\theta = 24.6°$. (b) The eigenfield distribution of corner state. (c)-(d) The eigenspectra and eigen field distribution of corner state in rhombus structure with introduced defects. (e)-(h) The eigenspectra and eigen field distribution of corner state in rhombus structure at $\theta = -34.2°$, and that with introduced defects.

We designed a rhombus structure with 10*10 cells, with a hard boundary. When $\theta = -34.2°$, Figs. 6(a)-(b) show the eigenfield distribution and eigenspectra. Similarly, Figs. 6(e)-(f) show these at $\theta =$

ISSN: 2414-1895 DOI: 10.6919/ICJE.202503_11(3).0011

24.6°. Both structures exhibit corner states at 21472 Hz, though the corner state appears in different positions for different θ. Adding defects by hollowing out three cells (replacing cell material with water in the simulation), as shown in Figs. 6(e)-(g), does not change the corner state or its frequency. This demonstrates the robustness of the rhombus structure at $\theta = -34.2°$ and $24.6°$.

8. Conclusion

In this paper, we designed a honeycomb structure capable of opening and closing band gaps. By rotating the crystal's scatterers around the center, we achieved band gap reversal, leading to a topological phase transition. When phononic crystals with different acoustic valley Hall phases are connected, sound field energy localizes at the interface, resulting in edge states. Triangular and rhombus structures yield corner states, which are topologically protected, robust, and related to the rotation angle. This structure has potential applications in filtering and rectifying acoustic signals in water.

References

[1] Y. Zhang, Y. Tan, H. L. Stormer, and P. Kim, Nature 438, 201 (2005). Doi: https://doi.org/10.1038/nature04235

[2] K. S. Novoselov, A. K. Geim, S. V. Morozov, D. Jiang, M. I. Katsnelson, I. V. Grigorieva, S. V. Dubonos, and A. A. Firsov, Nature 438, 197 (2005). Doi: https://doi.org/10.1038/nature04233

[3] A. H. Castro Neto, F. Guinea, N. M. R. Peres, K. S. Novoselov, and A. K. Geim, Rev. Mod. Phys. 81, 109 (2009). Doi: https://doi.org/10.1103/RevModPhys.81.109

[4] Liu J Y, Qiu C Y, Xu S J, et al. Dirac cones in two-dimensional artificial crystals for classical waves [J]. Physical Review B, 2014, 89 (13): 134302. Doi: https://doi.org/10.1103/PhysRevB.89.134302

[5] Herring, Conyers. Accidental Degeneracy in the Energy Bands of Crystals[J]. Phys Rev, 1937, 52(4):365-373.Doi: https://doi.org/10.1103/PhysRev.52.365

[6] Kazuaki Sakoda, "Dirac cone in two- and three-dimensional metamaterials," Opt. Express 20, 3898-3917 (2012). Doi: https://doi.org/10.1364/OE.20.003898

[7] Qi X L, Zhang S C 2011 Rev. Mod. Phys. 83 1057. Doi: https://doi.org/10.1103/RevModPhys.83.1057

[8] Hasan M Z, Kane C L 2010 Rev. Mod. Phys. 82 3045.Doi: https://doi.org/10.1103/RevModPhys.82.3045

[9] Bao J, Zou D, Zhang W, He W, Sun H, Zhang X 2019 Phys. Rev. B 100 201406(R) Doi: https://doi.org/10.1103/PhysRevB.100.201406

[10] Zheng S, Xia B, Man X, Tong L, Jiao J, Duan G, Yu D 2020 Phys. Rev. B 102 104113 Doi: https://doi.org/10.1103/PhysRevB.102.104113

[11] El Hassan A, Kunst F K, Moritz A, Andler G, Bergholtz E J, Bourennane M 2019 Nat. Photon. 13 697 Doi: https://doi.org/10.1038/s41566-019-0519-y

[12] Xie B Y, Su G X, Wang H F, Su H, Shen X P, Zhan P, Lu M H, Wang Z L, Chen Y F 2019 Phys. Rev. Lett. 122 233903. Doi: https://doi.org/10.1103/PhysRevLett.122.233903

[13] Peterson C W, Benalcazar W A, Hughes T L, Bahl G 2018 Nature 555 346 Doi: https://doi.org/10.1038/nature25777

[14] Serra-Garcia M, Peri V, Susstrunk R, Bilal O R, Larsen T, Villanueva L G, Huber S D 2018 Nature 555 342 Doi: https://doi.org/10.1038/nature25156

[15] Imhof S, Berger C, Bayer F, Brehm J, Molenkamp L W, Kiessling T, Schindler F, Lee C H, Greiter M, Neupert T, Thomale R 2018 Nat. Phys. 14 925 Doi: https://doi.org/10.1038/s41567-018-0246-1

[16] Xue H R, Yang Y H, Gao F, Chong Y D, Zhang B L 2019 Nature Materials 18 108 Doi: https://doi.org/10.1038/s41563-018-0251-x

[17] Ni X, Weiner M, Alù A, Khanikaev AB. Observation of Higher-Order Topological Acoustic States Protected by Generalized Chiral Symmetry. Nat Mater (2019) 18:113–20. Doi: https://doi.org/10.1038/s41563-018-0252-9

ISSN: 2414-1895 DOI: 10.6919/ICJE.202503_11(3).0011

[18] Xie B Y, Wang H F, Wang H X, Zhu X Y, Jiang J H, Lu M H, Chen Y F 2018 Phys. Rev. B 98 205147 Doi: https://doi.org/10.1103/PhysRevB.98.205147

[19] Xie B Y, Su G X, Wang H F, Su H, Shen X P, Zhan P, Lu M H, Wang Z L, Chen Y F 2019 Phys. Rev. Lett. 122 233903 Doi: https://doi.org/10.1103/PhysRevLett.122.233903

[20] Chen X D, Deng W M, Shi F L, Zhao F L, Chen M, Dong J W 2019 Phys. Rev. Lett. 122 233902 Doi: https://doi.org/10.1103/PhysRevLett.122.233902

[21] Fan H Y, Xia B Z, Tong L, Zheng S J, Yu D J 2019 Phys. Rev. Lett. 122 204301 Doi: https://doi.org/10.1103/PhysRevLett.122.204301

[22] Doi: https://doi.org/10.1063/1.5004073

[23] X. Huang, Y. Lai, Z. Hang, H. Zheng, and C. T. Chan, Nat. Mater. 10, 582 (2011). Doi: https://doi.org/10.1063/1.5004073

[24] F. Liu, Y. Lai, X. Huang, and C. T. Chan, Phys. Rev. B 84, 224113 (2011). Doi: https://doi.org/10.1103/PhysRevB.84.224113

[25] F. Liu, X. Huang, and C. T. Chan, Appl. Phys. Lett. 100, 071911 (2012). Doi: https://doi.org/10.1063/1.3686907

[26] I. Liberal and N. Engheta, Nat. Photonics 11, 149 (2017). Doi: https://doi.org/10.1038/nphoton.2017.13

[27] Y. Li, Y. Wu, and J. Mei, Appl. Phys. Lett. 105, 014107 (2014). Doi: https://doi.org/10.1063/1.4890304

[28] Z. Chen, M. Lu, Y. Wu, C. He, X. Sun, L. Zheng, M. Lu, and Y. Chen, Sci. Rep. 4, 4613 (2014). Doi: https://doi.org/10.1038/srep04613

[29] C. He, X. Ni, H. Ge, X. Sun, Y. Chen, M. Lu, X. Liu, and Y. Chen, Nat. Phys. 12, 1124 (2016).Doi: https://doi.org/10.1038/nphys3867

[30] J. Mei, Z. Chen, and Y. Wu, Sci. Rep. 6, 32752 (2016). Doi: https://doi.org/10.1038/srep32752

[31] L. Xu, H. Wang, Y. Xu, H. Chen, and J. Jiang, Opt. Express 24, 18059 (2016).Doi: https://doi.org/10.1364/OE.24.018059

[32] L. Zheng, Y. Wu, X. Ni, Z. Chen, M. Lu, and Y. Chen, Appl. Phys. Lett. 104, 161904 (2014).Doi: https://doi.org/10.1063/1.4873354

[33] DOI: 10.1103/PhysRevLett.126.156401

[34] A. Rycerz, J. Tworzydlo, and C. W. J. Beenakker, Valley filter and valley valve in graphene, Nat. Phys. 3, 172 (2007). Doi: https://doi.org/10.1038/nphys547

[35] D. Xiao, W. Yao, and Q. Niu, Valley-Contrasting Physics in Graphene: Magnetic Moment and Topological Transport, Phys. Rev. Lett. 99, 236809 (2007). Doi: https://doi.org/10.1103/PhysRevLett.99.236809

[36] J. Lu, C. Qiu, M. Ke, and Z. Liu, Valley Vortex States in Sonic Crystals, Phys. Rev. Lett. 116, 093901 (2016). Doi: https://doi.org/10.1103/PhysRevLett.116.093901

[37] J.-W. Dong, X.-D. Chen, H. Zhu, Y. Wang, and X. Zhang, Valley photonic crystals for control of spin and topology, Nat. Mater. 16, 298 (2017).Doi: https://doi.org/10.1038/nmat4807